Infrared absorption by molecular gases as a probe of nanoporous silica xerogel and molecule-surface collisions: Low-pressure results

J. Vander Auwera,[1] N. H. Ngo,[2] H. El Hamzaoui,[3] B. Capoen,[3] M. Bouazaoui,[3] P. Ausset,[2] C. Boulet,[4] and J.-M. Hartmann[2,*]

[1]*Service de Chimie Quantique et Photophysique, Code Postal 160/09, Université Libre de Bruxelles, 50 avenue F. D. Roosevelt, B-1050 Brussels, Belgium*

[2]*Laboratoire Interuniversitaire des Systèmes Atmosphériques (LISA), CNRS (UMR 7583), Universités Paris-Est Créteil et Paris Diderot, Institut P.-S. Laplace. Université Paris-Est Créteil, 94010 Créteil Cedex, France*

[3]*Laboratoire de Physique des Lasers, Atomes et Molécules (PhLAM), CNRS (UMR 8523), CERLA/IRCICA, Université de Lille 1, UFR de Physique Bâtiment P5, 59655 Villeneuve d'Ascq cedex, France*

[4]*Institut des Sciences Moléculaires d'Orsay (ISMO), CNRS (UMR 8214), Université Paris-Sud, Bâtiment 350, Orsay F-91405, France*

(Received 5 July 2013; published 14 October 2013)

Transmission spectra of gases confined (but not adsorbed) within the pores of a 1.4-cm-thick silica xerogel sample have been recorded between 2.5 and 5 μm using a high-resolution Fourier transform spectrometer. This was done for pure CO, CO_2, N_2O, H_2O, and CH_4 at room temperature and pressures of a few hectopascals. Least-squares fits of measured absorption lines provide the optical-path lengths within the confined (L^C) and free (L^F) gas inside the absorption cell and the half width at half maximum Γ^C of the lines of the confined gases. The values of L^C and L^F retrieved using numerous transitions of all studied species are very consistent. Furthermore, L^C is in satisfactory agreement with values obtained from independent measurements, thus showing that reliable information on the open porosity volume can be retrieved from an optical experiment. The values of Γ^C, here resulting from collisions of the molecules with the inner surfaces of the xerogel pores, are practically independent of the line for each gas and inversely proportional to the square root of the probed-molecule molar mass. This is a strong indication that, for the studied transitions, a single collision of a molecule with a pore surface is sufficient to change its rotational state. A previously proposed simple model, used for the prediction of the line shape, leads to satisfactory agreement with the observations. It also enables a determination of the average pore size, bringing information complementary to that obtained from nitrogen adsorption porosimetry.

DOI: 10.1103/PhysRevA.88.042506 PACS number(s): 33.70.Jg, 34.35.+a, 78.67.Rb, 81.20.Fw

I. INTRODUCTION

Nanoporous media are of great interest in materials science and they have several potential applications in many fields such as catalysis, gas storage, separation, sensing, optics, and biomedicine [1]. Since they are usually nontoxic, and chemically and thermally stable, inorganic nanoporous materials—which are mostly made of metal oxides—have been extensively employed as host materials. Sol-gel processes have been widely used in the synthesis of such inorganic materials. The main advantage is the possibility to obtain well-shaped samples with designed texture and composition at low processing temperatures [2]. For most practical applications, the determination of the textural properties of nanoporous materials is of crucial interest. Hence, several techniques have been developed in order to characterize the pore structure, such as electron microscopy, diffraction techniques, positron annihilation, mercury intrusion, and the widely used gas adsorption porosimetry [3–6]. However, according to [3], there is no method for the experimental determination of the absolute porosimetry parameters and the various characterization techniques provide only limited, albeit complementary information.

While many studies have investigated the spectra of molecules trapped in nanoporous media, focusing on the infrared signature of the adsorbed phase (e.g., [7–11] and references therein), little attention has been paid to gases less tightly confined and still free to move within the pores. Recent light-transmission experiments have been made only for one O_2 line in various ceramics [12–17] and some H_2O transitions within nanoporous alumina [14] and a silica aerogel [18] (note for completeness that confined atomic vapors have also been studied, as in [19–23], for instance). These studies show that the confinement induces a broadening of the absorption lines (e.g., [17,18]) that strongly depends on the pore size [16,17,24]. This behavior was quantitatively analyzed, for O_2 lines, using requantized classical molecular dynamics simulations [24]. Such optical soundings of gases within nanoporous media are of interest for two main reasons. The first is that the spectra show the signature of molecule-surface collisions and thus provide information on this process. The second is that some characteristics of the open porosity can also be obtained, as shown in the present paper and Refs. [12,16,24–26], making absorption measurements an interesting and complementary technique for the characterization of some porous materials.

This paper presents a study of the infrared absorption by CO, CO_2, N_2O, H_2O, and CH_4 gases confined, at room temperature and pressures of a few hectopascals (hPa), in a porous silica xerogel sample. The transmission spectra, recorded with a high-resolution Fourier transform spectrometer, have been analyzed through fits including the contribution of the free gas in the gaps between the sample and the absorption-cell windows and that of the gas within the open porosity of the xerogel. The two associated optical-path lengths are retrieved, together with the widths of the absorption lines of the confined

*Corresponding author: jean-michel.hartmann@lisa.u-pec.fr

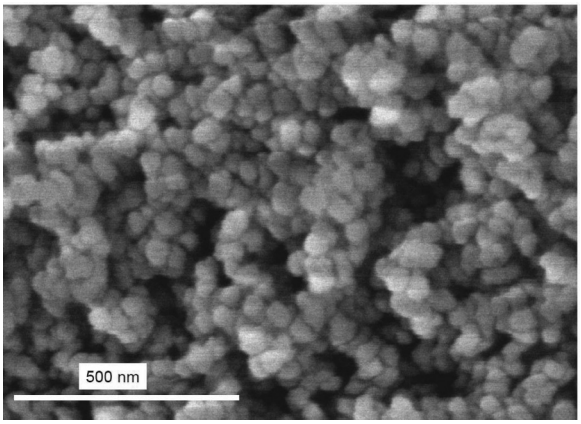

FIG. 1. Scanning electron microscope image of the silica xerogel sample surface.

gases. The results are first analyzed from the points of view of the porous volume and compared with determinations obtained with other techniques. The influence of molecule-wall collisions on the linewidths and line shapes are then described with a simple model. The latter leads to satisfactory agreement with the observations and provides information on the average pore size. The remainder of this paper is organized as follows. The silica xerogel sample is described in Sec. II and the infrared experiments and their treatment are the subjects of Sec. III. The results of the spectroscopic analysis of measured spectra are presented in Sec. IV and discussed in Sec. V.

II. SILICA XEROGEL SAMPLE

Various porous pure silica xerogels shaped as cylindrical rods, stabilized at 1000 °C and exhibiting interconnected pores, were prepared from tetraethylorthosilicate using the polymeric sol-gel technique reported in [27]. The sample used here has an almost cylindrical shape with a diameter $\Phi^{\text{Sample}} = 2.2 \pm 0.1$ cm, a thickness $L^{\text{Sample}} = 1.40 \pm 0.03$ cm, and thus a volume $V^{\text{Sample}} = 5.3 \pm 0.6$ cm^3. This sample was looked at using a scanning electron microscope with a magnification of 75 000 and sixteen photographs were taken, covering a total area of about 34 μm^2. As seen in the example of Fig. 1, the xerogel is composed of small silica grains with "entrance pores" of various sizes and shapes with a significant surface roughness. The analysis of the shape of about 230 of these grains indicates that they are almost spherical (average length- to-width ratio of 1:1) with a nearly Gaussian distribution of diameters centered at about 50 nm with a half width at half maximum of 8 nm.

For the characterization of the sample porosity, three independent measurements were made.

(i) In the first, the sample weight $w = 3.18$ g was determined and the empty volume V^{Empty} inside the sample was simply calculated from the relation $w = (V^{\text{Sample}} - V^{\text{Empty}})\rho$ where $\rho = 2.2$ g/cm^3 is the silica density. The relative open porosity determined by this weighting technique is then $p^{\text{Weight}} = 100V^{\text{Empty}}/V^{\text{Sample}} = 72\% \pm 4\%$. Note that since part of the empty volume inside the sample may not be accessible, this last value must be considered as an upper limit of the relative open porosity.

(ii) The second method is based on pressure and volume measurements in the absorption cell used (see Sec. III) for the infrared experiments. It was carried out as follows: A (poorly known) upstream volume V^{Up} inside a tube carrying a pressure gauge and connected to the cell but isolated from it by a valve, was filled up with He gas at a pressure P_0 while the cell was under vacuum. The valve was then opened to let the gas flow downstream and enter into the cell (the overall downstream volume being known as $V^{\text{Down}} = 13.3$ cm^3) and the pressure P_1 was measured. This enabled a precise determination of V^{Up} through $P_0V^{Up} = P_1(V^{Up} + V^{\text{Down}})$. Then exactly the same experiment was carried out after placing the xerogel sample into the cell and a pressure P_2 was measured. Assuming that the relative number of adsorbed molecules is negligible, this provides the volume V^{Closed}, within the xerogel sample, that is not accessible to the gas, through $P_0V^{Up} = P_2(V^{Up} + V^{\text{Down}} - V^{\text{Closed}})$. Since the overall volume V^{Sample} of the xerogel sample is known (see above), that of the open pores accessible to the gas is given by $V^{\text{Open}} = V^{\text{Sample}} - V^{\text{Closed}}$. This exercise, repeated for ten different initial He pressures between about 5 and 10 hPa, gives a relative open porosity of $p^{V+P} = 100 \times V^{\text{Open}}/V^{\text{Sample}} = 78\% \pm 3\%$. It is important to note that this method assumes that no He atoms are adsorbed on the sample surfaces. In fact, a relative amount of adsorbed atoms in the xerogel of only 2% leads to a relative porosity of 63%. Furthermore, the same pressure and volume experiment was carried out using CO gas, whose infrared spectrum within the xerogel sample shows a non-negligible adsorbed gas contribution. Using the same approach as for He, a relative porosity of 90% was obtained. This demonstrates that, due to a possible contribution of adsorption, the 78% relative open porosity obtained with He must be considered as an upper limit.

(iii) The third approach is based on nitrogen adsorption measurements at 77.35 K using a Quantachrome porosimeter Autosorb 1-LP-MP after an outgassing process of several hours at 150 °C under secondary vacuum. The specific surface area A was determined by the Brunauer-Emmett-Teller (BET) method [28], leading to $A = 130 \pm 2$ m^2/g. The total pore volume $V = 0.57 \pm 0.03$ cm^3/g was calculated from the volume of nitrogen adsorbed at a pressure close to the saturation vapor pressure. With the density $\rho = 2.2$ g/cm^3 for silica, the value of V leads to a relative open porosity $p^{\text{Ads}} = 55.6\% \pm 1.3\%$. Finally, a pore mean diameter of 24 nm was calculated using the desorption isotherm and the Barrett-Joyner-Halenda (BJH) formula [28], with a size distribution of width 15 nm, as shown in [27]. However, the isotherm shape diverges slightly from the conventional type IV, so that a macroporosity cannot be excluded [27]. Such a macroporosity is not taken into account in the BJH model.

The transmission of the xerogel in the infrared was also measured in order to determine which spectral region is appropriate for absorption experiments. This showed that the 14-mm-thick sample is opaque below about 2100 cm^{-1} but transmits radiations up to the visible. Note that, although the sample looks opaque and white, it scatters rather few visible radiations. Indeed, when illuminated by the focused light of a tungsten source, the circular spots on the front and back faces of the sample are very much alike. This implies that scattering in the infrared, for wavelengths more than four times greater than in the visible, plays a minor role.

TABLE I. Spectral range recorded ("Range"), as allowed by the bandpass filter ("Filter"), diameter of the entrance aperture of the FTS ("Iris") and maximum optical-path difference ("MOPD"; spectral resolution = 0.9/MOPD cm^{-1}) used, number of coadded interferograms ("Count"), average temperature (uncertainty = 1 K), and pressure used for the five species considered. Because of the fast evolution of the absorption resulting from the adsorption of water vapor in the xerogel, the 265 spectra recorded (each resulting from the coaddition of two interferograms) were treated separately; the minimum and maximum pressures are given. The uncertainties provided for the pressure are the square root of the sum of the square of half of the variation during the acquisition of the interferograms and the accuracy of measurement, conservatively estimated to be 0.5%.

	Range (cm^{-1})	Filter (cm^{-1})	Iris (mm)	MOPD (cm)	Count	T (K)	Pressure (hPa)
CH_4	2750–3250	–	0.8	225	684	294	9.911 (77)
H_2O	3500–4000	3300–4150	1.7	100	2 × 265	294	18.44(14)-23.85(12)
CO	2100–2260	2020–2500	1.5	225	484	294	5.30 (23)
N_2O	2140–2270	2020–2500	1.5	225	582	294	4.138 (50)
CO_2	2200–2420	2020–2500	1.5	225	528	294	0.965 (51)

III. INFRARED EXPERIMENTS AND THEIR ANALYSIS

A. Infrared measurements

The infrared transmissions were measured using a high-resolution (Bruker IFS 120 HR) Fourier transform spectrometer (FTS). The xerogel sample was inserted into a stainless-steel cylinder of length $L^{Cell} = 14.5 \pm 0.2$ mm closed by wedged CaF_2 windows. This cell was installed in the sample compartment of the evacuated FTS and connected by a $\frac{1}{4}$-in. tube to a gas handling and pumping system. The measurements were made at room temperature, stabilized by an air conditioning system. During the recordings of the interferograms, the temperature was monitored using two TSic 301 sensors (IST Innovative Sensor Technology; stated accuracy of ±0.3 K in the 10 °C–90 °C range) fixed onto the outer wall of the cell and the pressure was measured using (MKS Baratron model 690A) pressure gauges with full-scale ranges of 10 and 1000 Torr. For all experiments, the FTS instrument was equipped with a globar or tungsten source, an entrance aperture, a CaF_2 beam splitter, a low-pass or bandpass optical filter, and an InSb detector cooled down to 77 K. Finally, note that the optical arrangement of the FTS is such that the light that is transmitted through the cell is collected (by a mirror reflecting it toward the detector) within a solid angle of 0.08 sr only. Due to this very small value and to the moderate absorption and reflectance of silica in the studied infrared region, the contribution of scattered photons to the measured signals is likely negligible. We may thus consider that the light collected by the detector has gone straight through the xerogel sample.

In the experiments, the cell was first put under vacuum and a reference spectrum $I(\sigma, P = 0)$ was recorded versus the wavenumber σ. Gas was then admitted into the cell under a pressure P and, after a delay for stabilization, a second spectrum $I(\sigma, P)$ was collected. Finally, the cell was pumped out and a second reference spectrum was recorded in order to check (successfully in the present experiments) the stability of the signal. From these measurements, the transmission of the gas inside the cell (within and outside the xerogel sample) was obtained from $\tau^{Meas}(\sigma, P) = I(\sigma, P)/I(\sigma, P = 0)$. For water vapor, due to a strong adsorption, the cell was directly connected to a bottle of distilled water and the measurement was thus made at the liquid-vapor equilibrium pressure. Unapodized spectra of high-purity CH_4, H_2O, CO, CO_2, and N_2O were recorded using the above procedure for the experimental conditions listed in Table I.

A typical measured transmission, obtained for CO_2, is displayed in Fig. 2. At the scale of the plot, this spectrum looks very much like what would be observed for a free gas, except for the presence of the broad feature displayed in the inset. The analysis shows that its absorbance is proportional to the CO_2 pressure and peaks at about 2342 cm^{-1}, thus redshifted (–7 cm^{-1}) with respect to the free-gas band center (2349 cm^{-1} [29]). These characteristics indicate that it can be attributed, following [30–32], to the contribution of CO_2 molecules adsorbed on the pores' walls. Although an interesting subject, the analysis of this contribution, and of similar ones observed for the other molecules studied in this work, is beyond the scope of the present paper.

A closer look at individual lines, as exemplified by Fig. 3, shows that the measured spectrum involves two contributions, similar to those observed for H_2O in [18]. The narrow one is due to the free gas within the gaps (on both sides) between the xerogel sample and the absorption-cell windows. It results from the convolution of a narrow absorption line by the FTS instrument function. The former is essentially Doppler broadened since the collisional half width at half maximum

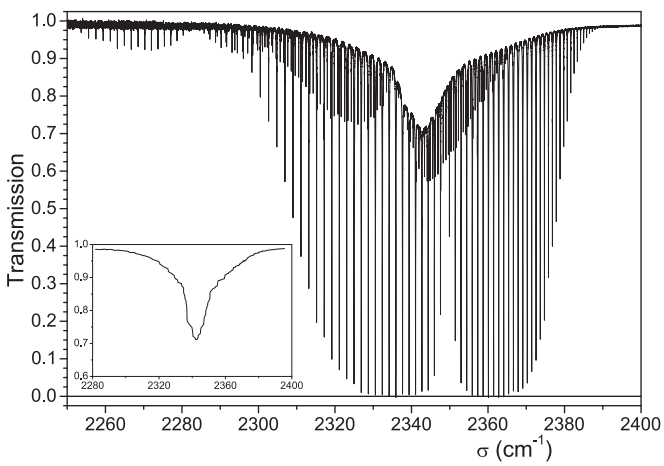

FIG. 2. Measured transmission spectrum of pure CO_2 in the region of the ν_3 band. The inset shows the adsorbed CO_2 contribution.

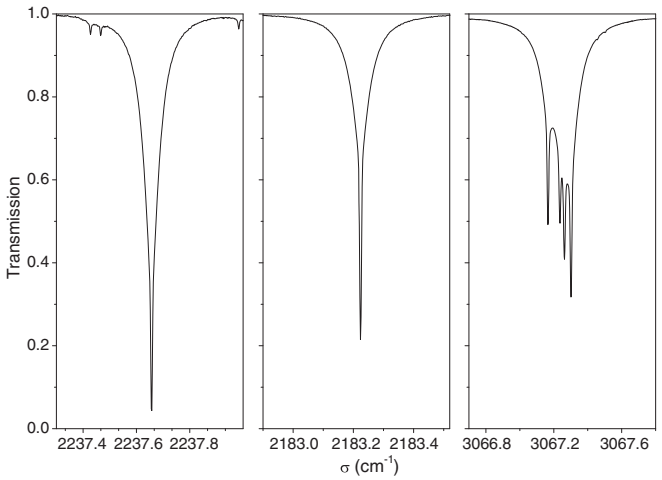

FIG. 3. Detailed views of measured transmission spectra. From left to right: the ν_3 band $R(17)$ line of N_2O at 4.14 hPa, the 1–0 band $R(10)$ line of CO at 5.29 hPa, and the ν_3 band $R(5)$ manifold of CH_4 at 9.91 hPa.

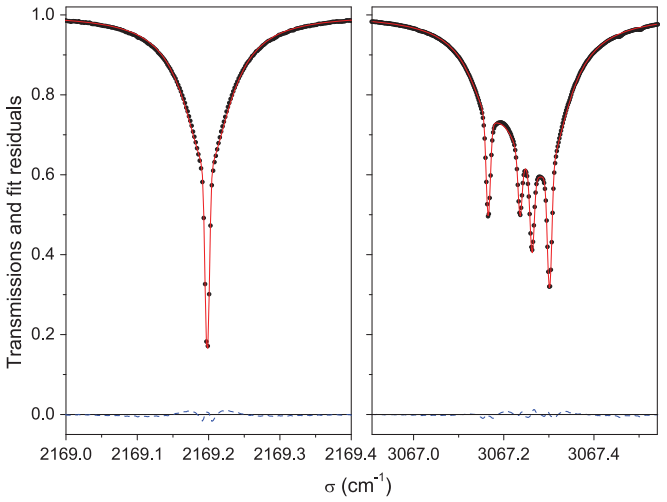

FIG. 4. (Color online) Transmission spectra of CO near the $R(6)$ line of the 1–0 band at 5.29 hPa (left) and of CH_4 near the $R(4)$ manifold of the ν_3 band at 9.91 hPa (right). The measured values (solid black circles) are compared with the fitted spectrum (red line), and the measured-fit residuals (dashed blue line) are displayed in the lower part of the plot.

(HWHM) at these low pressures is smaller [33] than 10^{-3} cm^{-1} (except for H_2O, for which the HWHM is about 0.01 cm^{-1} due to the large self-broadening coefficient and 20 hPa pressure used). The second contribution, that carries the former, is much broader (HWHM of 0.027–0.047 cm^{-1}; see Sec. IV) and has a nearly Lorentzian shape (Secs. III B and V C). It obviously cannot be explained, at the pressures of these experiments, by intermolecular collisions among molecules moving within the pores and thus mostly results from molecule-wall interactions.

B. Spectra analysis

Since the contribution of scattered photons can be neglected (see above), the measured infrared transmission of the not-adsorbed gas (free and within the xerogel) inside the absorption cell can be written, for a pressure P and a temperature T, as

$$\tau(\sigma,P,T) = \int_{-\infty}^{+\infty} F_{\text{Inst}}(\sigma-\sigma')\exp[-\alpha^F(\sigma',P,T)L^F - \alpha^C(\sigma',P,T)L^C]d\sigma'. \quad (1)$$

In this equation, $F_{\text{Inst}}(\cdots)$ is the FTS instrument function which can be calculated [34] from knowledge of the maximum optical-path difference and iris diameter used (see Table I). $\alpha^F(\sigma,P,T)$ and $\alpha^C(\sigma,P,T)$ are, respectively, the absorption coefficient of the free gas in the gaps between the xerogel sample and the cell windows and that of the gas confined within the xerogel pores. L^F and L^C are the corresponding averaged path lengths.

The absorption coefficient α^F of the free gas can be straightforwardly calculated by summing up the contributions of all optical transitions ℓ with Voigt shapes by using the line positions σ_ℓ, integrated intensities $S_\ell(T)$, and self-broadening coefficients $\gamma_\ell(T)$ given in the HITRAN database [33], i.e.,

$$\alpha^F(\sigma,P,T) = P\sum_{\text{lines }\ell} S_\ell(T)\text{VOIGT}\left[\sigma-\sigma_\ell,\Gamma_\ell^F(P,T),\Gamma_\ell^D(T)\right], \quad (2)$$

where $\Gamma_\ell^F(P,T) = P\gamma_\ell(T)$ and $\Gamma_\ell^D(T)$ is the Doppler HWHM. This calculation provides results with an accuracy better than 5% according to the stated uncertainties [33] of the spectroscopic parameters used.

For the contribution α^C of the gas moving within the xerogel pores, a similar expression is used but, considering the significant broadening induced by molecule-wall collisions (e.g., Fig. 3), the influence of the Doppler effect is negligible and a Lorentzian line shape is used. This is an approximation (see Fig. 4, Sec. V C and [24]) but sufficiently valid for a reliable determination of the path lengths and lines' HWMHs. α^C is thus expressed as

$$\alpha^C(\sigma,P,T) = P\sum_{\text{lines }\ell}\frac{S_\ell(T)}{\pi}\frac{\Gamma_\ell^C(P,T)}{\left[\sigma-\sigma_\ell-\Delta_\ell^C(P,T)\right]^2+\Gamma_\ell^C(P,T)^2}, \quad (3)$$

where Γ_ℓ^C and Δ_ℓ^C are, respectively, the HWHM and spectral shift of line ℓ due to the molecules' collisions with the inside walls of the pores.

The measured spectra have been least-squares fitted using Eqs. (1)–(3) by floating the values of L^F, L^C, Γ_ℓ^C, and Δ_ℓ^C, while all other parameters (σ_ℓ, S_ℓ, Γ_ℓ^F, and Γ_ℓ^D) have been computed from the parameters provided by the HITRAN database [33]. This was done using adequate microwindows around each optical transition or manifold. A linear law $a\sigma+b$ multiplying the experimental transmissions was also introduced for each fitting window in order to correct for the absorption background (due to adsorbed molecules, nearby lines, and/or experimental biases). For the methane ν_3-band manifolds, which involve closely spaced transitions, the same value of Γ_ℓ^C and Δ_ℓ^C was assumed for all lines. Furthermore, line-mixing effects [35], clearly evidenced in free-CH_4 spectra [36–38], are disregarded by Eq. (3). The quality of the fits (e.g., Fig. 4) indicates that these two approximations are very reasonable, a result that will be discussed in a forthcoming

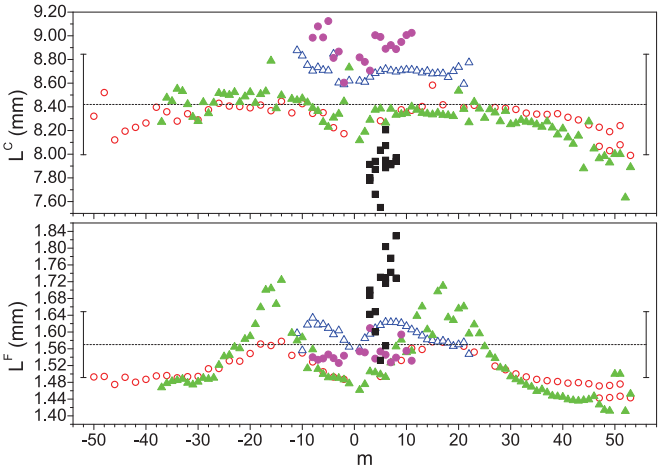

FIG. 5. (Color online) Optical-path lengths within the free gas (L^F, bottom) and the gas confined in the xerogel (L^C, top) obtained from fits of various lines in the low-pressure spectra of CH_4 (full magenta circles), H_2O (full black squares), CO (open blue triangles), CO_2 (open red circles), and N_2O (full green triangles). The results are plotted versus the rotational quantum number m of the line (or manifold) such that $m = J + 1$ for $R(J)$ lines and $m = -J$ for $P(J)$ lines. The dashed line gives the overall averaged value and the error bars indicate the $\pm 5\%$ interval.

paper. Typical examples of measured-spectra fits are plotted in Fig. 4, showing the quality of the adjustments.

IV. RESULTS

A. Path lengths

The values of L^F and L^C deduced from the fits of numerous lines in the spectra of all studied molecules are displayed in Fig. 5. The results are consistent since the values are (as they should be) almost independent of the gas and of the optical transition. With respect to the overall averaged values $\bar{L}^F = 1.57$ mm and $\bar{L}^C = 8.42$ mm; differences for individual lines and absorbing species remain lower than 14% and 8%, respectively. A part of the differences between the results retrieved from lines of different molecules can be attributed to uncertainties on the spectroscopic data used (from 2% to 5% according to [33]). Remaining inconsistencies likely come from experimental uncertainties and from the use, in the fits, of approximate descriptions of both the instrument function and line shape. Note that the results, particularly those for L^F, show systematic dependences versus the rotational quantum number m. These changes of L^F with m are very similar to those of the line intensities with maxima near $|m| \simeq 16$ for CO_2 and N_2O and $|m| \simeq 8$ for CO. Since the relative line intensities within a band are accurately known, the observed variations of L^F for a given gas cannot be attributed to inconsistencies in the spectroscopic data. The reason for them is the fact that the fits of the free-gas contribution are not perfect (Fig. 4), here essentially due to a small error in the description of the FTS instrument function since the line profile, being almost Doppler, is well known. This introduces a bias in the retrieved L^F that depends on how much the considered line absorbs and thus on the line intensity. The overall results obtained for all gases and lines, synthesized in Table II, confirm the high consistency of the spectroscopic determinations of the optical paths.

B. Linewidths

Before discussing the linewidths Γ^C, let us mention that the fits show no evidence of any detectable spectral shift Δ_ℓ^C for all studied lines and molecules. This could be expected due to the likely small differences between the molecule-surface interaction potentials in the quite close lower and upper vibrational states of the considered transitions. It is nevertheless in contrast with those obtained for H_2O in [18] where significant spectral displacements of the lines were observed. Possible explanations for this are the facts that, in this previous study, lines at higher frequencies were studied and that the pore size was significantly smaller.

The values of Γ^C for numerous transitions in the spectra of all studied molecules are displayed in Fig. 6. They have been obtained from those determined in the fits by subtracting the contribution $\Gamma_\ell^F(P,T)$ of intermolecular collisions (only significant for H_2O). They thus entirely result from molecule-wall collisions. Obviously, Γ^C is practically independent of the transition for each gas (with scatters from $\pm 3\%$ for CO to $\pm 7\%$ for H_2O) but it significantly depends on the absorbing species. Note that, when the HWHM is multiplied by the square root of the molecular mass, the resulting value becomes (see Table II) independent of the molecule. These original results are analyzed in the next section.

V. DISCUSSION

A. Confined path length and porous volume

For the length of the path within the open pores inside the xerogel sample, the average of all optical determinations

TABLE II. Average optical-path lengths in the free (L^F) and confined (L^C) gases and HWHMs (Γ^C) of the confined gases lines deduced from fits of measured spectra (see text). M is the molar mass, P is the average pressure of the measurements, N_L is the number of lines (manifolds for methane) used, and ΔJ gives the min and max values of the initial rotational quantum number J for the studied transitions. The mean values are given with the corresponding standard deviations (in units of the last digit) inside parentheses.

Gas	M (g)	P (hPa)	N_L	ΔJ	Band	L^F (mm)	L^C (mm)	Γ^C (cm^{-1})	$\Gamma^C\sqrt{M}$ (g$^{1/2}$/cm)
CH_4	16	9.91	18	0–10	ν_3	1.55(02)	8.91(13)	0.0469(11)	0.187
H_2O	18	22.7	16	1–6	ν_3	1.71(10)	7.90(15)	0.0445(17)	0.188
CO	28	5.29	33	1–22	1–0	1.59(02)	8.70(07)	0.0338(04)	0.179
CO_2	44	0.965	50	0–53	ν_3	1.51(04)	8.31(12)	0.0273(06)	0.181
N_2O	44	4.14	89	0–53	ν_3	1.53(08)	8.32(18)	0.0276(09)	0.183

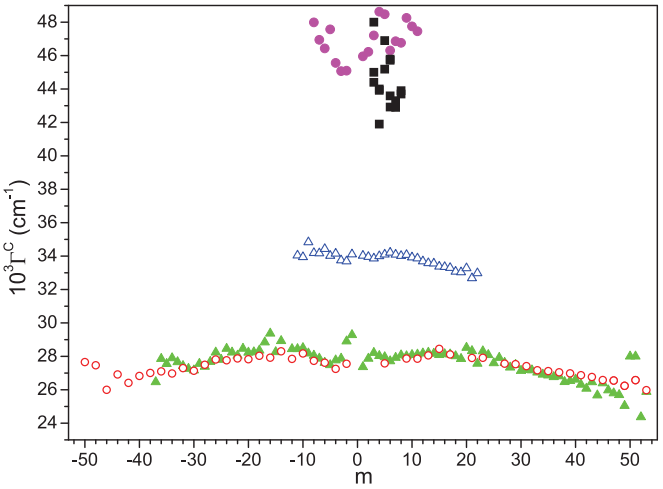

FIG. 6. (Color online) HWHMs due to molecule-wall collisions obtained from fits of various lines in the spectra of confined CH_4 (full magenta circles), H_2O (full black squares), CO (open blue triangles), CO_2 (open red circles), and N_2O (full green triangle). The results are plotted versus the rotational quantum number m of the line (or manifold) such that $m = J + 1$ for $R(J)$ lines and $m = -J$ for $P(J)$ lines.

shown in Fig. 5 and Table II is $\bar{L}^C = 8.4 \pm 0.6$ mm, leading to an optically determined porosity $p^{\text{Opt}} = 100\bar{L}^C/L^{\text{Sample}} = 60\% \pm 5\%$. This value is in very satisfactory agreement with that ($p^{\text{Ads}} = 55.6\% \pm 1.3\%$) determined using nitrogen adsorption porosimetry. It is also compatible with the upper limits obtained (see Sec. II B) from the sample weight and volume ($p \leqslant p^{\text{Weight}} = 72\% \pm 4\%$) and from the pressure and volume measurements ($p \leqslant p^{V+P} = 78\% \pm 3\%$). Hence, for porous samples made of a material (here silica) transparent to infrared radiation so that the collected photons have followed a straight path, the porosity can be retrieved from transmission measurements. This is not the case for ceramics, for instance, in which the photons exiting the back face of the sample have been scattered many times and have traveled average optical paths much longer than the sample thickness [15].

B. Linewidths and pore size

The HWHMs Γ^C due to molecule-wall collisions are, for each absorbing species, practically independent of the transition (Fig. 6 and Table II). The efficiency of the molecule-wall collisions in broadening the line is thus independent (for those studied) of the (initial) rotational state of the molecule as it heads toward the wall. The only possible explanation for this behavior is that a single collision is sufficient to change the molecule rotation (i.e., the quantum number J for a linear molecule) and interrupt the radiation process. This is consistent with the theoretical analysis of [24] and, if it were not the case, since changing J gets more and more difficult as J increases, the HWHM should be significantly smaller for high J than for low J, as observed in free gas (the pressure-broadening coefficients vary by nearly a factor of 2 from $J = 1$ to 20 for pure CO [39] and from $J = 1$ to 50 for pure CO_2 [40], for instance).

If we neglect the Doppler effect (valid here since $\Gamma^D \ll \Gamma^C$), the area-normalized absorption coefficient of an isolated line centered at the angular frequency $\omega_\ell = 2\pi c\sigma_\ell$ is

$$\alpha(\omega) = \frac{1}{\pi}\text{Re}\left\{\int_0^{+\infty} e^{i(\omega_\ell-\omega)t}\frac{N(t)}{N(0)}dt\right\}, \tag{4}$$

where $N(t)$ is the number of molecules initially absorbing on the considered transition at $t = 0$ which still absorb at time t. When a single collision with a pore wall removes the molecule from its initial rotational state, $N(t)$ is obviously the number of molecules which have not hit a wall between times 0 and t. If we also assume that the molecule-surface interaction potential is an infinitely steep repulsive wall, a simple model can be derived. Indeed, using Boltzmann statistics for translational velocities and a spatially uniform distribution of molecules within a parallelepipedic box of side lengths L_x, L_y, and L_z, and following the developments of Appendix A of [24] and of references cited therein, one has

$$\frac{N(t)}{N(0)} = \frac{N_x(t)}{N_x(0)}\frac{N_y(t)}{N_y(0)}\frac{N_z(t)}{N_z(0)}$$

with, in the case of the x axis, for instance,

$$\frac{N_x(t)}{N_x(0)} = \frac{1}{L_x}\int_{-L_x/2}^{+L_x/2} dx \int_{-(L_x/2+x)/t}^{(L_x/2-x)/t} f_{MB}(v_x)dv_x$$

$$\text{and} \quad f_{MB}(v) = \sqrt{\frac{M/N_A}{2\pi k_B T}}e^{-\frac{Mv^2}{2N_A k_B T}}, \tag{5}$$

with M the molar mass, N_A the Avogadro number, and k_B the Boltzmann constant. Recall that one has [41]

$$\frac{N_x(t)}{N_x(0)} = \text{erf}\left[\sqrt{\frac{M}{2N_A k_B T}}\frac{L_x}{t}\right] - \frac{t}{L_x}\sqrt{\frac{2N_A k_B T}{\pi M}}\left[1 - \exp\left(-\frac{M}{2N_A k_B T}\frac{L_x^2}{t^2}\right)\right]. \tag{6}$$

If we assume that this function can be approximated by an exponential decay having the same slope $\frac{1}{N_x(0)}\frac{dN_x}{dt}(0) = -\sqrt{(2N_A k_B T)/(\pi M)}/L_x$ at $t = 0$ and if we introduce this exponential into Eq. (4), the line then has a Lorentzian shape with a HWHM of

$$2\pi c \times \Gamma^C(\text{cm}^{-1}) = \sqrt{\frac{2N_A k_B T}{\pi M}}\left[\frac{1}{L_x} + \frac{1}{L_y} + \frac{1}{L_z}\right] = (A/V)\sqrt{\frac{N_A k_B T}{2\pi M}}, \tag{7}$$

where A is the parallelepipedic enclosure inner area and V is its volume (a result previously obtained in [42]). In order to go further, absorption coefficients have been calculated using Eqs. (4)–(6) for various enclosures with $L_x = L_y \ll L_z$ and fitted using Lorentzian profiles. The HWHMs obtained with this more rigorous procedure are only slightly larger that those predicted by Eq. (7), confirming, after [24], that this equation is reliable. Hence, the HWHM due to molecule-wall collisions is, within the proposed model, independent of the optical transitions and proportional to $1/\sqrt{M}$. These two predictions are in agreement with experiments since Fig. 6 demonstrates

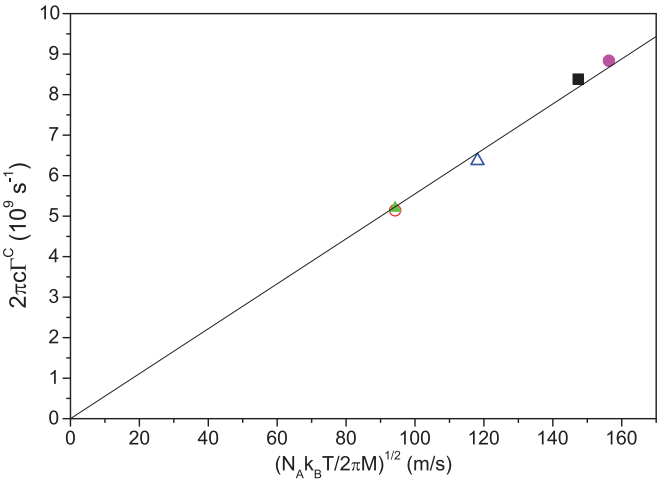

FIG. 7. (Color online) Averaged HWHMs due to molecule-wall collisions obtained from fits of the spectra of confined CH_4 (full magenta circles), H_2O (full black squares), CO (open blue triangles), CO_2 (open red circles), and N_2O (full green triangles) plotted versus the velocity involved in Eq. (7). The size of the symbols corresponds to a $\pm 2\%$ uncertainty and the straight line has a slope of 0.0555 nm^{-1}.

the line independence while Table II and Fig. 7 confirm the mass dependence. This reinforces the assumption of the full efficiency of a single molecule-wall collision in changing the rotational state.

At this step note that, in the case of a cylinder of length L and diameter d, one has $A/V = 4/d$ and, introducing the mean speed $\bar{v} = \sqrt{(8N_A k_B T)/(\pi M)}$, the half width is, according to Eq. (7),

$$2\pi c \times \Gamma^C(\mathrm{cm}^{-1}) = \bar{v}/d. \tag{8}$$

The validity of this last equation was proved in [24] using requantized molecular dynamics simulations and experimental results (in references therein) for the broadening of an O_2 absorption line in various ceramics with pores of different sizes. It also seems a good approximation in view of the measurements for four H_2O lines (in air) confined in alumina presented in [14]. In that study, the averaged HWHM due to molecule-wall collisions (difference between the observed value and that for free gas) is 0.045 cm^{-1}. Using Eq. (8), this value leads to $d = 69.6$ nm which is in excellent agreement with the 70 nm value deduced [14] from mercury intrusion porosimetry. Finally, again for H_2O, wall-collision-broadened HWHMs from 0.20 to 0.32 cm^{-1} were observed in a silica aerogel [18]. Equation (8) then leads to pore diameters between 15 and 10 nm, significantly smaller than the stated value of 20 nm. Note that large line-to-line variations of the confined gas HWHMs were found in [18], in opposition with our results. This may result from the much looser confinement in our xerogel sample.

From Fig. 7 and Eq. (7), the A/V ratio can be deduced from a linear law fit, leading to the optically determined value of $(A/V)^{\mathrm{Opt}} = 0.055 \pm 0.002$ nm^{-1} which, in the case of a cylinder, corresponds to a diameter of $d = 73$ nm. While $(A/V)^{\mathrm{Opt}}$ is about four times smaller than the value $(A/V)^{\mathrm{Ads}} = 0.228 \pm 0.013$ nm^{-1} determined by nitrogen adsorption (see Sec. II), it is important to note that the involved areas A do not represent the same quantity. Indeed, while the nitrogen adsorption technique measures the true overall area of the inside surface of the pores, the optical measurements determine the somehow projected area. The first includes the contribution of the local surface roughness but the second does not. Hence, the ratio $A^{\mathrm{Ads}}/A^{\mathrm{Opt}}$ is necessarily greater than unity and can be of several units if the fractal dimension of the surface is large. As an illustrative but very crude example, consider a long and wide (along x and y) parallelepipedic box of height $L_z = 140$ nm ($L_z \ll L_x$ and $L_z \ll L_y$) whose inner surface is covered by very closely spaced cubes of side length $l = 50$ nm (the diameter of the silica grains; see Sec. II and Fig. 1). In this case, the inside volume is $V \approx L_x L_y (L_z - 2l)$ and the total surface area for adsorption is $A^{\mathrm{Ads}} = 5l^2(2L_x L_y/l^2)$. Thus $(A/V)^{\mathrm{Ads}} \approx 10/(L_z - 2l)$ and the A/V ratio as determined optically is $(A/V)^{\mathrm{Opt}} \approx 2/(L_z - 2l)$. With the numbers given above, we get $(A/V)^{\mathrm{Opt}} \approx 0.05\,\mathrm{nm}^{-1}$ and $(A/V)^{\mathrm{Ads}} \approx 0.25\,\mathrm{nm}^{-1}$ which are close to the measured ones (0.055 and 0.228 nm^{-1}, respectively). We can also imagine a situation with a much smaller-scale surface roughness, as in a L_x-long cylinder of diameter $d \ll L_x$ whose inner surface is covered by closely spaced cubes of side length $l \ll d$. In this case, $(A/V)^{\mathrm{Ads}} \approx 20/d$ and $(A/V)^{\mathrm{Opt}} \approx 4/d$ which, for $d = 80$ nm again leads to values of 0.05 and 0.25 nm^{-1}, close to the measured ones. The two above given examples are obviously far too simple but they show that very different pore structures can lead to similar values of the (A/V) ratios. In fact, a consistent modeling of the fractal structure would be extremely hazardous, as nothing is known about the exact pore shapes and about their interconnections. Furthermore, the gas adsorption technique cannot be used to estimate the contribution of macropores, which apparently exist in the scanning electron microscope (SEM) image of Fig. 1. However, the previous simple calculations show that the discrepancies between the estimated pore diameters obtained by gas adsorption and by optical spectroscopies can be qualitatively explained by surface roughness and macroporosity.

C. Line shapes

In order to quantify how the line shapes of confined gases deviate from the Lorentzian (or Voigt if the Doppler contribution is significant) profile, we have taken the Naperian logarithm of the observed transmissions and divided it by the absorbance at the center of the absorption contribution due to the confined gas. After this transformation, used in [24,43], for instance, the measured-fit residuals are expressed relative to the peak absorption value. The results obtained are exemplified in Figs. 8(top) and 8(bottom). If one "visually" removes [as exemplified by the blue curve in Fig. 8(top)] the narrow central dip due to the slightly improper modeling of the free-gas contributions, the fit residuals have a W-shaped signature. This last finding, which is well known for free gas [35], expresses a line-narrowing due to velocity changes and to the speed dependence of the collisional relaxation rates. The minimum and maximum values of the residuals in Figs. 8(top) and 8(bottom) range from about -0.03 to $+0.05$ and the overall amplitudes of the W's are between 6% and 8% for the molecules studied. This result confirms the fact, observed

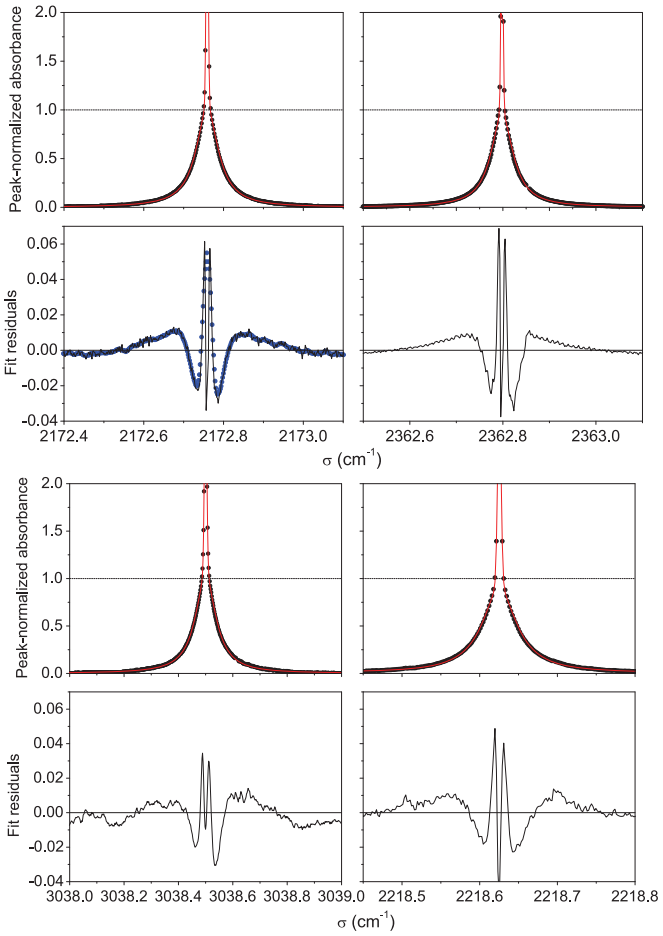

FIG. 8. (Color online) (top) Observed (full black circles) and fitted (red line) peak-normalized line shapes (top panels) and measured-fit residuals (lower panels, black line) for the 1–0 band $R(7)$ line of CO (left) and ν_3 band $R(18)$ line of CO_2 (right). The full blue circles in the lower left panel show the residuals after a "handmade" removal of the central dip. (bottom) Same as (top) but for the ν_3 band $R(1)$ line of CH_4 (left) and ν_3 band $P(6)$ line of N_2O (right).

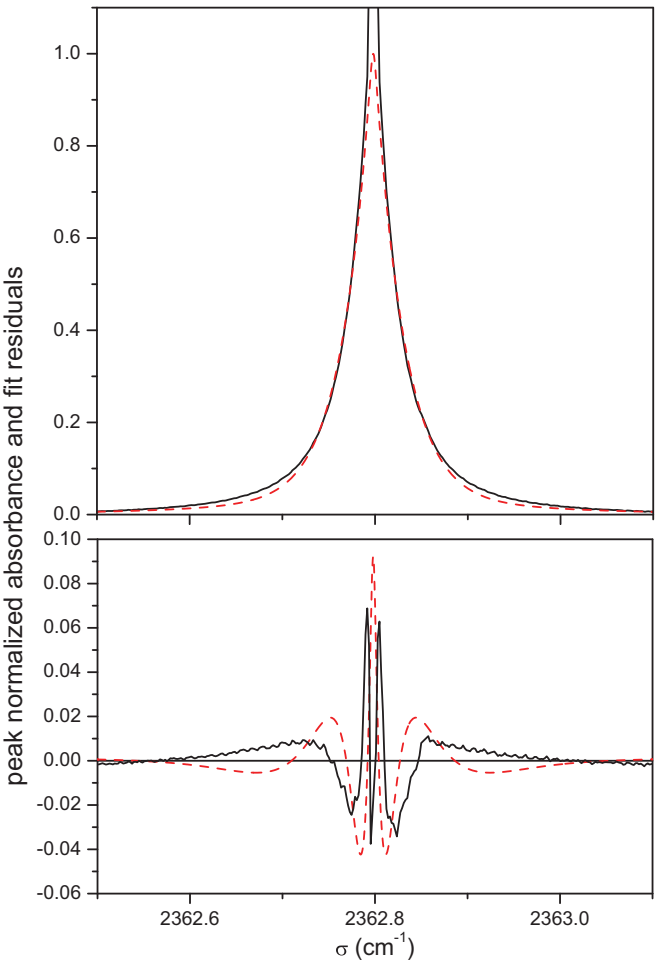

FIG. 9. (Color online) Peak-normalized absorbances (top) and Lorentzian-fit residuals (bottom) for the $R(18)$ line of CO_2. The black lines and red dashed lines have been obtained from measured and calculated (see text) spectra, respectively.

in [24] for O_2, that the confinement induces a narrowing of the line with respect to a Lorentz (or Voigt) profile several times larger than that due to intermolecular collisions in free gas. Indeed, the average 7% amplitude observed here is to be compared with the values, all below 3%, obtained under free-gas conditions for pure CO_2 [43], N_2O [44], CO [45], H_2O [46,47], and CH_4 [48].

Calculations have also been made using Eqs. (4)–(6) for CO_2 molecules inside an infinitely long parallelepipedic enclosure of square cross section (i.e., $L = L_x = L_y \ll L_z$). The value of L was adjusted in order to obtain a line HWHM identical to the experimental one (0.027 cm^{-1}) and the obtained profile was fitted with a Lorentzian shape. This leads to the results plotted in Fig. 9 together with similar ones obtained using the measured $R(18)$ line. The model leads, despite its great simplicity, to a semiquantitative agreement with experiments. For more rigorous predictions, molecular dynamics simulations, as done in [24], must be made and this will be the subject of a forthcoming paper. Finally, note that one cannot rule out a contribution of the pore-size and -shape distributions to the observed line shape. If we assume, for instance, a material with two pore types corresponding to equally distributed cylinders of diameters d and $d/4$, the resulting line profile will be the superposition of two nearly Lorentzian shapes of HWHMs, $\bar{\nu}/(2\pi cd)$ and $4\bar{\nu}/(2\pi cd)$, respectively. Its fit with a single Lorentzian profile would obviously lead to significant residuals. In order to go a little further, we have simulated, using Eqs. (4)–(6), the profile for $L_0 = L_x = L_y = 73\,\text{nm} \ll L_z$ and compared it with that resulting from a Gaussian distribution of parallelepipedic pores of square section $L = L_x = L_y \ll L_z$ centered at $L = L_0$ and of HWHM $L_0/2$. The Lorentzian fits of these two profiles lead to very similar residuals showing that the influence of the pore size distribution is, for the Gaussian one retained, almost negligible.

VI. CONCLUSION

This paper presents recordings and analyses of infrared spectra of low-pressure CO, CO_2, N_2O, H_2O, and CH_4 gases

moving inside the pores of a 14-mm-thick silica xerogel nanoporous cylinder. The fits of these spectra provide the line half widths due to the collisions of the molecules with the inner surface of the pores and the optical-path length within the confined gases. The results show a noticeable independence of the retrieved path length on the gas and on the optical transition used for its determination. Furthermore, the optically obtained value leads to a relative porosity in good agreement with that determined by other means. Concerning the linewidths, they also are independent of the transition for a given gas and are proportional to $1/\sqrt{M}$, where M is the molecule molar mass. These findings support the idea that a single collision of a molecule with the pore inside surface is sufficient to change its rotational state. Within this frame, a relation between the linewidth and the average size of the pores is obtained, information completing that obtained from nitrogen adsorption porosimetry, which demonstrates the interest of optical soundings of porous materials. Finally, a simple model has been used for the prediction of the line shape that leads to satisfactory predictions of the observed significant deviations between the measured wall-collision-broadened line shapes and the Lorentzian profile. Further studies of interest would be to investigate the influence of the xerogel structure (pore size) and of the gas pressure on the observed absorption shapes. Such topics will be the subject of our future works.

ACKNOWLEDGMENTS

The authors from PhLAM thank the Conseil Régional du Nord-Pas de Calais and the Fonds Européen de Développement Régional for their support through the Contrat de Projets Etat Région (Contract No. 2007-2013) and the Campus Intelligence Ambiante. J.V.A. acknowledges financial support from the Fonds de la Recherche Scientifique (F.R.S.-FNRS, Belgium) and the Action de Recherches Concertées of the Communauté française de Belgique.

[1] Q. Xu, *Nanoporous Materials: Synthesis and Applications* (CRC Press, Boca Raton, FL, 2013).
[2] C. J. Brinker and G. W. Scherer, *Sol-Gel Science* (Academic Press, New York, 1990).
[3] J. Rouquerol, D. Avnir, C. W. Fairbridge, D. H. Everett, J. H. Haynes, N. Pernicone, J. D. F. Ramsay, K. S. W. Sing, and K. K. Unger, Pure Appl. Chem. **66**, 1739 (1994).
[4] S. Polarz and B. Smarsly, J. Nanosci. Nanotechnol. **2**, 581 (2002).
[5] M. Thommes, Chem. Ing. Tech. **82**, 1059 (2010).
[6] P. Wong, *Methods of the Physics of Porous Media* (Academic Press, San Diego, 1999).
[7] E. Cohen de Lara, Phys. Chem. Chem. Phys. **1**, 501 (1999).
[8] G. Hubner, G. Rauhut, H. Stoll, and E. Roduner, Phys. Chem. Chem. Phys. **4**, 3112 (2002).
[9] N. Zvereva-Loëte, A. Ballandras, G. Weber, M. Rotger, V. Boudon, and J.-M. Simon, Mol. Phys. **107**, 2081 (2009).
[10] M. Sanzharov, M. Rotger, M. Loete, V. Boudon, N. Zvereva-Loete, A. Ballandras, and G. Weber, J. Chem. Phys. **136**, 134314 (2012).
[11] E. Garrone and C. Otero Arean, Chem. Soc. Rev. **34**, 846 (2005).
[12] T. Svensson, M. Andersson, L. Rippe, J. Johansson, S. Folestad, and S. Andersson-Engels, Opt. Lett. **33**, 80 (2008).
[13] T. Svensson and Z. Shen, Appl. Phys. Lett. **96**, 021107 (2010).
[14] T. Svensson, M. Lewander, and S. Svanberg, Opt. Express **18**, 16460 (2010).
[15] T. Svensson, E. Adolfsson, M. Lewander, C. T. Xu, and S. Svanberg, Phys. Rev. Lett. **107**, 143901 (2011).
[16] T. Svensson, E. Adolfsson, M. Burresi, R. Savo, C. T. Xu, D. S. Wiersma, and S. Svanberg, Appl. Phys. B **110**, 147 (2013).
[17] C. T. Xu, M. Lewander, S. Andersson-Engels, E. Adolfsson, T. Svensson, and S. Svanberg, Phys. Rev. A **84**, 042705 (2011).
[18] Y. N. Ponomarev, T. M. Petrova, A. M. Solodov, and A. A. Solodov, Opt. Express **18**, 26062 (2010).
[19] C. Andreeva, S. Cartaleva, L. Petrov, S. M. Saltiel, D. Sarkisyan, T. Varzhapetyan, D. Bloch, and M. Ducloy, Phys. Rev. A **76**, 013837 (2007).
[20] G. Dutier, P. Todorov, I. N. Hamdi, I. Maurin, S. Saltiel, D. Bloch, and M. Ducloy, Phys. Rev. A **72**, 040501 (2005).
[21] P. Ballin, I. Maurin, A. Laliotis, and D. Bloch, in *CLEO/Europe and EQEC 2011 Conference Digest* (Optical Society of America, Washington, DC, 2011), p. EI_P6.
[22] S. Cartaleva, S. Saltiel, A. Sargsyan, D. Sarkisyan, D. Slavov, P. Todorov, and K. Vaseva, J. Opt. Soc. Am. B **26**, 1999 (2009).
[23] C. Perrella, P. S. Light, J. D. Anstie, T. M. Stace, F. Benabid, and A. N. Luiten, Phys. Rev. A **87**, 013818 (2013).
[24] J.-M. Hartmann, V. Sironneau, C. Boulet, T. Svensson, J. T. Hodges, and C. T. Xu, Phys. Rev. A **87**, 032510 (2013).
[25] G. Somesfalean, M. Sjöholm, J. Alnis, C. af Klinteberg, S. Andersson-Engels, and S. Svanberg, Appl. Opt. **41**, 3538 (2002).
[26] L. Mei, S. Svanberg, and G. Somesfalean, Opt. Express **20**, 16942 (2012).
[27] H. El Hamzaoui, L. Courthéoux, V. N. Nguyen, E. Berrier, A. Favre, L. Bigot, M. Bouazaoui, and B. Capoen, Mater. Chem. Phys. **121**, 83 (2010).
[28] S. Brunauer, P. H. Emmett, and E. Teller, J. Am. Chem. Soc. **60**, 309 (1938).
[29] L. S. Rothman, R. L. Hawkins, R. B. Wattson, and R. R. Gamache, J. Quant. Spectrosc. Radiat. Transfer **48**, 537 (1992).
[30] M. Fastow, Y. Kozirovski, and M. Folman, J. Electron. Spectrosc. Relat. Phenom. **64-65**, 843 (1993).
[31] W.-L. Yim, O. Byl, J. John, T. Yates, and J. K. Johnson, J. Chem. Phys. **120**, 5377 (2004).
[32] C. Matranga, L. Chen, M. Smith, E. Bittner, J. K. Johnson, and B. Bockrath, J. Phys. Chem. B **107**, 12930 (2003).
[33] L. S. Rothman, I. E. Gordon, A. Barbe, D. C. Benner, P. F. Bernath, M. Birk, V. Boudon, L. R. Brown, A. Campargue, J.-P. Champion, K. Chance, L. H. Coudert, V. Dana, V. M. Devi, S. Fally, J.-M. Flaud, R. R. Gamache, A. Goldman, D. Jacquemart, I. Kleiner *et al.*, J. Quant. Spectrosc. Radiat. Transfer **110**, 533 (2009).

[34] S. P. Davis, M. C. Abrams, and J. W. Brault, *Fourier Transform Spectrometry* (Academic Press, San Diego, 2001).
[35] J.-M. Hartmann, C. Boulet, and D. Robert, *Collisional Effects on Molecular Spectra. Laboratory Experiments and Models, Consequences for Applications* (Elsevier, Amsterdam, 2008).
[36] D. Pieroni, Nguyen-Van-Thanh, C. Brodbeck, C. Claveau, A. Valentin, J.-M. Hartmann, T. Gabard, J.-P. Champion, D. Bermejo, and J.-L. Domenech, J. Chem. Phys. **110**, 7717 (1999).
[37] H. Tran, P.-M. Flaud, T. Gabard, F. Hase, T. von Clarmann, C. Camy-Peyret, S. Payan, and J.-M. Hartmann, J. Quant. Spectrosc. Radiat. Transfer **101**, 284 (2006).
[38] H. Tran, J.-M. Hartmann, G. Toon, L. R. Brown, C. Frankenberg, T. Warneke, P. Spietz, and F. Hase, J. Quant. Spectrosc. Radiat. Transfer **111**, 1344 (2010).
[39] A. Predoi-Cross, C. Hnatovsky, K. Strong, J. R. Drummond, and D. Chris Benner, J. Mol. Struct. **695-696**, 269 (2004).
[40] A. Predoi-Cross, A. V. Unni, W. Liu, I. Schofield, C. Holladay, A. R. W. McKellar, and D. Hurtmans, J. Mol. Spectrosc. **245**, 34 (2007).
[41] P. E. Wagner, R. M. Somers, and J. L. Jenkins, J. Phys. B **14**, 4763 (1981).
[42] M. Danos and S. Geschwind, Phys. Rev. **91**, 1159 (1953).
[43] J.-M. Hartmann, H. Tran, N. H. Ngo, X. Landsheere, P. Chelin, Y. Lu, A.-W. Liu, S.-M. Hu, L. Gianfrani, G. Casa, A. Castrillo, M. Lepère, Q. Delière, M. Dhyne, and L. Fissiaux, Phys. Rev. A **87**, 013403 (2013).
[44] F. Rohart, J.-M. Colmont, G. Wlodarczak, and J.-P. Bouanich, J. Mol. Spectrosc. **222**, 159 (2003).
[45] J. W. Brault, L. R. Brown, C. Chackerian, Jr., R. Freedman, A. Predoi-Cross, and A. S. Pine, J. Mol. Spectrosc. **222**, 220 (2003).
[46] N. H. Ngo, H. Tran, and R. R. Gamache, J. Chem. Phys. **136**, 154310 (2012).
[47] H. Tran, N. H. Ngo, J.-M. Hartmann, R. R. Gamache, D. Mondelain, S. Kassi, A. Campargue, L. Gianfrani, A. Castrillo, E. Fasci, and F. Rohart, J. Chem. Phys. **138**, 034302 (2013).
[48] M. Lepère, J. Mol. Spectrosc. **238**, 193 (2006).